Quantitative Assessment of System Response during Disruptions
An Application to Water Distribution Systems

Cassottana, Beatrice; Aydin, Nazli Yonca; Tang, Loon Ching

DOI
10.1061/(ASCE)WR.1943-5452.0001334

Publication date
2021

Document Version
Final published version

Published in
Journal of Water Resources Planning and Management

Citation (APA)
Cassottana, B., Aydin, N. Y., & Tang, L. C. (2021). Quantitative Assessment of System Response during Disruptions: An Application to Water Distribution Systems. *Journal of Water Resources Planning and Management*, *147*(3), Article 04021002-1. https://doi.org/10.1061/(ASCE)WR.1943-5452.0001334

Quantitative Assessment of System Response during Disruptions: An Application to Water Distribution Systems

Beatrice Cassottana[1]; Nazli Yonca Aydin[2]; and Loon Ching Tang[3]

Abstract: The resilience of water distribution systems (WDSs) has gained increasing attention in recent years. Various performance loss and recovery behaviors have been observed for WDSs subject to disruptions. However, a model for their characterization, which could provide further insight for resilience assessment and enhancement, is still lacking. Here, the authors develop a recovery function to model WDS performance over time following a disruption. This function is useful to compare system responses under different disruption and recovery scenarios and supports the identification of areas for improvement within various aspects of the resilience of a WDS. The proposed model was applied to two benchmark networks. Different scenarios were analyzed in which one node at a time was disrupted and two recovery strategies were implemented. It was found that the developed model supports the implementation of tailored strategies to improve WDS resilience according to the location of the disruption, therefore enhancing the efficient allocation of resources. **DOI: 10.1061/(ASCE)WR.1943-5452.0001334.**

Introduction

The resilience of water distribution systems (WDSs) has gained increasing attention in recent years, as the impact of climate change, urbanization, cascading failures, and uncertainty due to the growing interdependence among critical infrastructures has escalated to an alarming level. Currently, a standard model for assessing WDS resilience in various disruption and recovery scenarios is still lacking, thus hampering its application to real case studies. In the literature, resilience metrics for WDSs have been classified into two groups: attribute-based and performance-based (Diao et al. 2016).

Attribute-based resilience metrics (also referred to as graph-based resilience metrics) are defined using the tools of network theory. Algebraic connectivity, clustering coefficient, average path length, and other topological metrics have been used as proxies for WDS resilience (Yazdani et al. 2011; Porse and Lund 2015; Meng et al. 2018). Hybrid metrics also have been developed to simultaneously account for topology and hydraulic variables, where weights were given to the nodes or the links of the graph (Herrera et al. 2015; Yazdani and Jeffrey 2012). Although those metrics represent an effort to broaden the scope of topological metrics by including hydraulic variables, they addressed resilience from a structural perspective and ignored the complex dynamics governing the behavior of WDSs.

Performance-based metrics have relied on the performance observed in the output of hydraulic models, i.e., pressure inside the system, satisfied demand, and water quality (Aydin 2018; Cimellaro et al. 2015; Diao et al. 2016). Resilience was then quantified in terms of performance loss (Amarasinghe et al. 2016), time to recovery (Mabrouk et al. 2010; Khatavkar and Mays 2019), or both (Mugume et al. 2015; Diao et al. 2016; Klise et al. 2017; Butler et al. 2017). Additionally, Cimellaro et al. (2015) computed the expected performance loss over time using the well-known resilience triangle (Bruneau et al. 2003). Overall, performance-based metrics provide a comprehensive evaluation of resilience for WDSs, because these metrics result from the complex interactions between structural and hydraulic variables, as modeled by the simulation software. However, most metrics have quantified system states only at certain points of time, typically at the time of maximum performance loss and at the moment of recovery. This did not enable comparison among systems presenting similar performance loss and time to recovery, but which express different behaviors.

In order to conduct comparative studies, recovery functions are used to model the time-continuous system response during the entire duration of a disruption, including periods of loss and restoration of performance. Existing recovery functions were either developed according to some parametric and time-dependent models or were empirically based on available data. In the former case, different functional forms were assumed, and the parameters were estimated through curve-fitting techniques, such as minimizing the sum of squares. Exponential recovery functions were found to fit well to the recovering performance of critical infrastructures, including power (Chang 1998; Reed et al. 2010), transport (Comes and Van de Walle 2014), and health care (Cimellaro et al. 2010) systems. However, those functions ignored the performance loss process. Therefore, in order to represent both performance loss and recovery, Todman et al. (2016) developed a recovery function in analogy with a mechanical spring damper system, while Cassottana et al. (2019) proposed families of recovery functions with parameters capable of representing key characteristics of recovery processes. Although these models have proven useful for assessing and comparing resilience, they could only model fast performance losses followed by relatively slower recoveries. However, there is still a need for modeling various performance loss and recovery behaviors, including slow performance losses followed by relatively faster recoveries.

[1]Postdoctoral Researcher, Singapore-ETH Centre, 1 Create Way, CREATE Tower #06-01, Singapore 138602 (corresponding author). ORCID: https://orcid.org/0000-0001-5856-9361. Email: beatrice.cassottana@frs.ethz.ch

[2]Assistant Professor, Faculty of Technology, Policy and Management, Delft Univ. of Technology, Jaffalaan 5, Delft 2628 BX, Netherlands. Email: n.y.aydin@tudelft.nl

[3]Professor, Dept. of Industrial Systems Engineering and Management, National Univ. of Singapore, Singapore 117576. Email: isetlc@nus.edu.sg

Note. This manuscript was submitted on January 29, 2020; approved on September 19, 2020; published online on January 12, 2021. Discussion period open until June 12, 2021; separate discussions must be submitted for individual papers. This paper is part of the ***Journal of Water Resources Planning and Management***, © ASCE, ISSN 0733-9496.

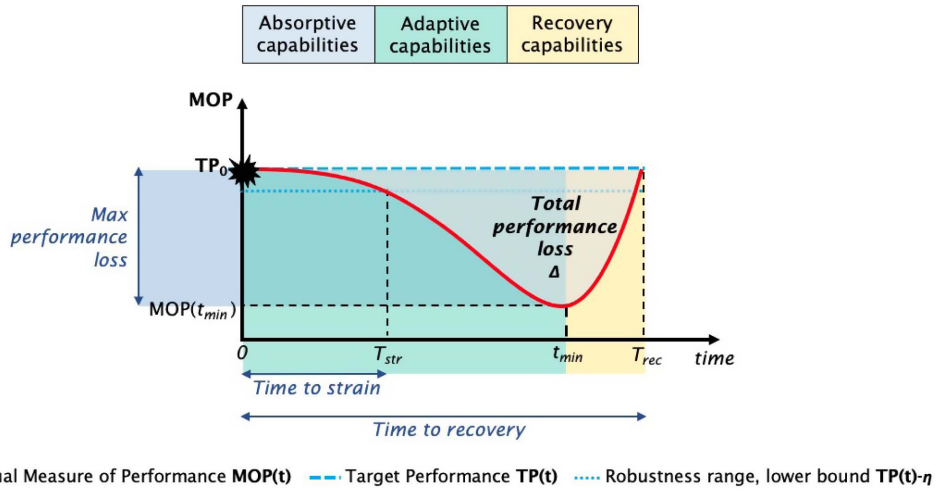

Fig. 1. Time-continuous system response during a disruption.

With application to WDSs, those behaviors were simply represented using empirical data. Specifically, previous literature shows that, for WDSs subject to certain types of disruptions, slow performance losses and fast recoveries are observed. Brentan et al. (2018), for example, observed slow pressure losses for a WDS subject to nodal leaks at certain locations. Tarani et al. (2019) found that the loss of performance, measured in terms of demand deficiency over time, was delayed with respect to the start of a flood wave, and that it was quickly recovered following system restoration. Similarly, Cimellaro et al. (2015) assumed a two-step response for a WDS subject to pipe bursts, characterized by a delayed loss of performance, i.e., number of households with water, and a sudden recovery following complete restoration. Davis (2014) analyzed the restoration of the Los Angeles WDS following the 1994 Northridge earthquake. In that case, the water delivery service was quickly restored to 80% of its target level soon after the end of the earthquake. Finally, Meng et al. (2018) found strong correlation between failure magnitude and recovery rate, possibly due to the fact that recovery shortly followed pipe restoration. Overall, empirical evidence from previous studies show that WDS behavior is determined by many factors, such as the type of disruption and the monitored measure of performance. Currently, these behaviors have been simply evaluated using empirical data (Shen et al. 2020), and a model for their characterization, which could provide further insight for resilience assessment and enhancement, is still lacking.

This paper develops a new recovery function that is capable of modeling various performance loss and recovery behaviors, including slow/fast losses of performance followed by faster/slower recoveries, and whose parameters are capable of representing key characteristics of recovery processes. The function developed is therefore selected to model the behavior of a WDS subject to pipe bursts, which is characterized by slow performance losses followed by relatively faster recoveries. With further analysis of the function parameters, groups of scenarios are identified, in which the system exhibits similar response behaviors and which can be easily labeled to support decisions to improve WDS resilience before and during a disruption. To the best of the authors' knowledge, this is the first study to assess WDS resilience and corresponding recovery strategies using recovery functions. We apply the developed model to analyze the resilience of two benchmark networks, i.e., *Net3* and *C-Town*, and different disruption scenarios are simulated as water leakages due to pipe bursts at different locations. We find that the developed model supports the identification of characteristic system behaviors as well as the development of tailored resilience strategies to improve WDS performance, thereby enhancing the efficient allocation of resources.

Methods

Time-Continuous System Response

The time-continuous system response during a disruption is represented in Fig. 1. System response is determined by different variables, including the external disruption process and the intrinsic capabilities of the system (Shen et al. 2020). These include absorptive capability (i.e., the ability to minimize the impacts of disruptions), adaptive capability (i.e., the ability to self-organize for recovery of performance), and recovery capability (i.e., the ability of a system to be repaired) (Vugrin et al. 2011).

Initially, the system functions at its target performance (TP) level and is perturbed by an external shock at time $t = 0$. If the system is able to adapt to the shock, the performance is maintained within the robustness range and performance loss (or strain) is delayed until $t = T_{str}$, when the performance reaches the lower bound of the robustness range (TP $- \eta$). Consequently, the system performance drops until it reaches the minimum performance level MOP_{min} at $t = t_{\text{min}}$. The magnitude of the maximum incurred performance loss (PL), which is equal to $\text{TP} - \text{MOP}(t_{\text{min}})$, depends upon the severity of the disruption as well as the absorptive capability of the system (Vugrin et al. 2011; Meng et al. 2018). However, the time to strain (T_{str}) and the rate of performance loss, i.e., the amount of MOP lost per unit of time, are determined by the adaptive capability of the system, according to the concept of graceful degradation (Woods 2015). When the effects of the recovery efforts take place to reduce the consequences of the disruption, system performance begins to recover and is eventually restored to the initial level TP at $t = T_{rec}$. Therefore, the recovery rate, i.e., the amount of MOP restored per unit of time, and the time to recovery (T_{rec}) will be determined by the recovery capabilities of the system (Vugrin et al. 2011). In a nutshell, the system response to a disruption depends upon the extent to which the system can absorb, adapt to, and recover from it.

Moreover, the total performance loss Δ, which is the cumulative performance loss over the entire duration of the disruption, has been often used to provide a summary information of the overall

system resilience (the lower the Δ, the higher the resilience of the system) (Bruneau et al. 2003):

$$\Delta = \int_0^{T_{rec}} [\mathrm{TP}(t) - \mathrm{MOP}(t)]dt \tag{1}$$

Recovery Functions for Response Modeling

In order to model the time-continuous system response, we fit recovery functions to the measure of performance. A recovery function is a parametric function that maps t to MOP, i.e., $\mathrm{MOP}(t)$: $t \mapsto \mathrm{MOP}$. Here, the beta family of recovery functions is developed to model the time-continuous system response:

$$\mathrm{MOP}(t) = \begin{cases} \mathrm{TP} - a\dfrac{(b+c)^{b+c}}{b^b c^c}\left(\dfrac{t}{\nu}\right)^b\left(1-\dfrac{t}{\nu}\right)^c & \text{if } 0 \le t \le \nu \\ \mathrm{TP} & \text{otherwise} \end{cases} \tag{2}$$

where TP is the target performance level and a, b, c and ν are parameters to be estimated, with $0 \le a \le 1$ and $b, c, \nu \ge 0$. The expression of the recovery function in Eq. (2) is motivated by the need to represent various recovery processes, which differ in terms of maximum performance loss, rate of performance loss, rate of restoration, and time to recovery. The term $(b+c)^{b+c}/(b^b c^c)$ is a normalization factor that enables a better physical interpretation of the function parameters. Closed-form solutions exist for the maximum performance loss, $\mathrm{TP} - \mathrm{MOP}(t_{\min}) = 1 - a$, and for the time to recovery, $T_{rec} = \nu$.

Versatility of the Beta Family of Recovery Functions

The beta family of recovery functions in Eq. (2) is versatile in representing different system responses. Various performance losses can be modeled according to location parameter a, and different rates of loss/restoration can be modeled according to shape parameters b, c and time scale parameter ν. In Fig. S1, the characteristic behaviors of the beta family of recovery functions based on various combinations of the parameters b and c are identified. Although this family can only represent a return to the predisruption performance level, it can model both symmetric and asymmetric recovery processes, including fast performance losses followed by a relatively slower recovery and slow performance losses followed by a relatively faster recovery. Specifically, the case $b = c$ corresponds to symmetric recovery processes, $b > c$ corresponds to slow performance losses followed by a relatively faster recovery, and $b < c$ corresponds to fast performance losses followed by a relatively slower recovery.

Physical Interpretation of the Beta Family of Recovery Functions

The physical interpretation of the function parameters helps to assess the extent to which the system is able to absorb, adapt to, and recover from a disruption. The parameters of the beta family characterize performance and time quantities. The two effects are separated, with a characterizing performance quantities, and b, c and ν characterizing time quantities. Location parameter a equals the magnitude of the maximum incurred performance loss, as shown in Fig. 2(a), which depends upon the severity of the adverse event and the extent to which the system absorbs the disruption. Time scale parameter ν equals the time to recovery, as shown in Fig. 2(b), which depends upon the duration of the disruptive event and the extent to which the system is able to timely recover. Shape parameters b and c determine the shape of the system behavior during periods of performance loss and restoration.

Shape parameters are of utmost importance, because they control the performance rate and the convexity of the curve, which provide further insight for resilience assessment. Existing resilience metrics quantify the average rates of performance loss and restoration as the ratio of maximum performance loss to a certain time quantity, i.e., $\mathrm{PL}/t_{\min}$ or PL/T_{rec} (Meng et al. 2018). However, rate is a time-dependent variable, which is not easily captured using empirical data alone (its value should be computed at each time point). Shape parameters b and c solve this problem by characterizing different shapes and providing summary information on how the performance loss rate changes over time.

Specifically, parameter b characterizes the performance loss behavior, as shown in Fig. 2(b): $b \le 1$ characterizes behaviors with short time to strain and sudden loss of performance; $b > 1$ characterizes behaviors with long time to strain and delayed loss of performance. A long time to strain and a low performance loss rate ($b > 1$) correspond to high-performing adaptive capabilities.

Parameter c characterizes the recovery behavior, as shown in Fig. 2(c): $c \le 1$ characterizes behaviors with delayed recovery and performance suddenly approaching TP later in time; $c > 1$ characterizes behaviors with timely recovery and performance approaching TP asymptotically. The earlier performance starts to recover and approaches TP ($c > 1$), the earlier the system recovers its functionalities. Therefore, high values of c correspond to enhanced recovery capabilities.

Overall, the physical interpretation of the beta function brings further insight into the resilience of the system by associating the function parameters to different response behaviors, therefore supporting the identification of areas for improvement within various aspects of resilience.

Simulated Disruption and WDS Performance

Disruptions to the network are here simulated as pipe bursts. To model a pipe burst, a sudden leakage flow is added to the demand nodes (Brentan et al. 2018). In order to identify the critical nodes of the network without relying on predisruption hypotheses related to their locations, an $n-1$ analysis is conducted: given a network with n demand nodes, we consecutively disrupt the ith node, with $i = 1, \ldots, n$, and we study the behavior of the system relying on the $n-1$ remaining nodes. During the disruption, the nodal leak demand (d_i^{leak}) is proportional to the magnitude of the disruption, i.e., the area of the hole (A), and the nodal pressure p_i, as modeled by Crowl and Louvar (2001):

$$d_i^{leak}(t) = C_d A\sqrt{\frac{2p_i(t)}{\rho}} \tag{3}$$

where C_d is the discharge coefficient assumed to be 0.75 (turbulent flow), and ρ is the density of the water. As a consequence of the additional flow due to the leak demand, the nodal pressure decreases, with a detrimental effect on the demand served (d_i), as modeled by the pressure-demand relationship:

$$d_i(t) = \begin{cases} 0 & p_i(t) \le P_0 \\ D_i(t)\left(\dfrac{p_i(t)-P_0}{P_f-P_0}\right)^{0.5} & P_0 \le p_i(t) \le P_f \\ D_i(t) & p_i(t) \ge P_f \end{cases} \tag{4}$$

where D_i is the desired demand at node i (m^3/s), P_f is the nominal pressure assumed to be 20 m, and P_0 is the lower pressure threshold assumed to be 0 m, below which the consumer cannot receive any water. Because the WDS is designed to operate at a pressure greater

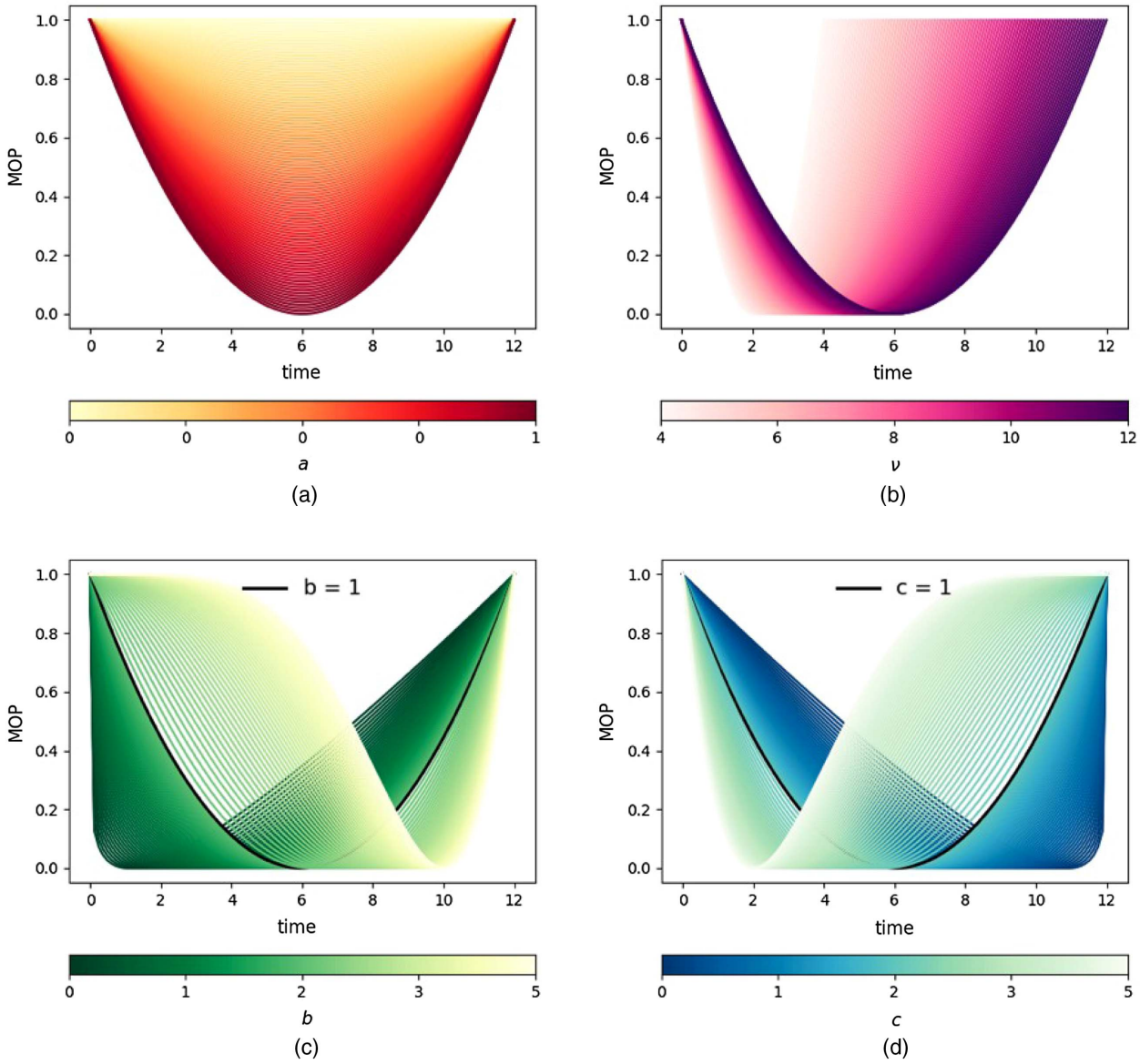

Fig. 2. Effect of parameter (a) a; (b) ν; (c) b; and (d) c on the beta family of recovery functions.

than or equal to the nominal pressure P_f, according to Eq. (4) in normal conditions the served demand equals the desired demand. However, if a disruption occurs, then part of the desired demand might remain unsatisfied not only at the disrupted node, but also at the nodes connected to it, which might also suffer pressure losses to compensate for the additional flow. Therefore, the time-dependent demand served d_i is a direct consequence of the intrinsic capacities of the WDS in terms of pressure built up and damage sustained (pressure loss) (Shen et al. 2020). Accordingly, here the average satisfied demand is used as a proxy for the demand delivery service to monitor the overall system performance when node i is disrupted:

$$\text{MOP}_d^{(i)}(t) = \frac{1}{n}\sum_{i=1}^{n}\frac{d_i(t)}{D_i(t)} \tag{5}$$

Note that in Eq. (5), i is used as superscript to denote the overall system performance following the disruption of node i and as a subscript to denote the demand of each node $i, i = 1, \ldots, n$ in the network. Because by design the served demand equals the desired demand in normal conditions, TP equals 1. In order to compute performance under different disruption scenarios, pressure-dependent demand hydraulic simulations are run using the Water Network Tool for Resilience (WNTR) (Klise et al. 2017) implemented in Python 3.7.

Recovery Function Selection

For WDSs subject to individual component failures, i.e., water leakages, relatively slower losses in the demand delivery service followed by sudden recoveries are observed. Other disruptions, such as multiple pipe failures, would result in a sudden loss of performance and could be modeled using the recovery functions developed in Cassottana et al. (2019) as discussed in the Introduction. During water leakages, however, WDSs can still meet a certain level of water demand thanks to their distributed water tanks and stand-by pumping capacity (Diao et al. 2016). Valves can also be installed to isolate failed components, in order to prevent cascading failures in the network (Cimellaro et al. 2015). The more redundancies and buffer capacity the WDS has, the more it can

adapt to a disruption, resulting in delayed losses of service. Following losses, the full service is restored at the time instant following the end of the disruption. In fact, no lags are observed between the restoration of the disrupted component and the recovery of the entire system.

While existing recovery functions only model fast losses of performance followed by slower recoveries, the beta family of recovery functions is versatile in representing slow/fast losses of performance followed by faster/slower recoveries, and it is therefore employed in this study. Specifically, the case of slow performance losses followed by a faster recovery is characterized by the parameters relationship $b > c$. Because recovery to TP occurs suddenly and late in time, the shape of the recovery behavior is characterized by $c \leq 1$. Therefore, the two characteristic behaviors that will be observed in this study correspond to (1) $b, c \leq 1$; with $b > c$ and (2) $b > 1, c \leq 1$. Behavior (2) corresponds to higher adaptive capabilities ($b > 1$), since performance loss is delayed in time, and it is therefore preferred to enhance system resilience.

Because recovery to TP immediately follows the end of the disruption, T_{rec} is known in advance according to the simulated disruption duration. As a result, the restoration rate is linearly correlated with the maximum performance loss (Meng et al. 2018). In view of the above considerations, the parameter of the beta family ν is set to $\nu = T_{rec}$. The recovery capabilities of the system are therefore not analyzed further, since they are fully determined by the simulation inputs.

Node Clustering

The parameters a and b of the beta recovery function characterize the extent to which the WDS is able to absorb and adapt to a water leakage (since the recovery capabilities are fixed given the simulation inputs, parameters c and ν are not considered for the analysis). In order to prioritize the efforts in recovery, we select q nodes, which are the most critical based on the total performance loss in Eq. (1). We then characterize the ith node based on the system response following its disruption as modeled by the beta recovery function, i.e., based on the estimated parameters a_i and b_i, with $i = 1, \ldots, q$. We cluster the q nodes using the well-known k-means algorithm. Given the set of estimated parameters $\{(a_1, b_1), \ldots, (a_q, b_q)\}$, the algorithm aims at partitioning the q nodes into $K < q$ clusters $\{C_1, \ldots, C_K\}$ by minimizing the sum of the squared distances:

$$\min_{\{C_1,\ldots,C_K\}} \sum_{k=1}^{K} \sum_{i \in C_k} (a_i - a_k, b_i - b_k)^2 \tag{6}$$

where (a_k, b_k) is the average position of cluster k, i.e., centroid:

$$(a_k, b_k) = \left(\frac{1}{|C_k|} \sum_{i \in C_k} a_i, \frac{1}{|C_k|} \sum_{i \in C_k} b_i \right) \tag{7}$$

The resulting clusters $\{C_1, \ldots, C_K\}$ denote groups of nodes whose disruption results in a similar response behavior and could therefore be used by system operators to create tailored emergency plans and guide investment to improve resilience.

When deciding on the number of clusters K, a trade-off exists between the accuracy with which the clusters represent the nodes and the amount of resources that can be effectively managed and deployed to address the disruptions in each clusters. While a higher number of clusters accurately represents the nodes, a lower number of clusters can be effectively labeled and used to develop tailored resilience strategies (Brentan et al. 2018). Ultimately, the system operators will decide on the optimal number of clusters based on the results of the clustering algorithm and on the available resources. Here, in order to evaluate the performance of the clustering algorithm, the sum of the squared distances of the nodes to their assigned centroid (intra-distance criterion) is plotted against increasing values of K and the optimal number of clusters is selected according to the so-called elbow of the curve. The elbow of the curve is the value after which improvements in the objective function become smaller. Other indices could be used to evaluate the performance of the clustering algorithm, e.g., the Calinski-Harabaz index used by Brentan et al. (2018), which increases with the distance among clusters (interdistance criterion) and decreases with the sum of the squared distances. However, since overlaps among clusters increase WDS resilience, here we only use the intradistance criterion.

Case Studies

Benchmark WDSs and Disruption Scenarios

Two benchmark WDSs were analyzed in this study, *Net3* and *C-Town*. *Net3* is relatively smaller, with 97 nodes and 119 links, compared to *C-Town*, with 396 nodes and 444 links. *Net3* has two reservoirs, one of which operates only part of the day, and three water tanks with a total capacity of 28,633 m^3, which serve an average daily demand of 62,576 m^3. *C-Town* has one reservoir and seven water tanks with a total capacity of 9,501 m^3, which are operated through 11 water pumps and serve an average daily demand of 15,452 m^3. While *Net3* represents a large-scale WDS at a low resolution, *C-Town* represents a WDS at a local scale and high resolution. This is also evident in the network topology metrics [see Yazdani et al. (2011) for a definition of average path length and clustering coefficient]. The high average path length (l_T) of *Net3* ($l_T = 2.45$) reveals long routes for traversing this network (i.e., large scale), whereas *C-Town* is characterized by short routes ($l_T = 0.13$). Moreover, the clustering coefficient (c_c) suggests that *C-Town* is less connected than *Net3* ($c_c = 0.03$ and 0.04, respectively), showing a more distributed and localized distribution.

The disruptions were assumed to start at the time of the peak demand and to last 24 h. This assumption was aligned with previous literature, which assumed a time to recovery of 1–2 days, and was justified by the fact that major water leakages are typically easily detected few hours after their occurrence (Cimellaro et al. 2010; Klise et al. 2017). The 24-h period allowed analysis of WDS resilience on different demand periods based on the daily demand pattern. Additionally, it was assumed that repairs to leaking components were conducted without interrupting service. In practice, this could be achieved through local isolation, if this is possible without disrupting the entire network, or using hot tapping and welding (McReynolds and Peng 2012; Herckis 2018). For the two networks, the magnitude of the disruption A was set to 0.06 m^2 for *Net3* and to 0.02 m^2 for *C-Town*. These values produced similar performance losses for the two networks after normalizing the leak demand based on their respective average water demand. For each network, an $n-1$ analysis was conducted, where one node at a time was disrupted, with t_0, T_{rec}, and A fixed. The $n-1$ analysis produced a total of n scenarios for each network, which differed according to the location of the disruption.

In order to validate the robustness of the results, a design of experiment was conducted for *Net3* in which t_0, T_{rec}, A and the location of the disruption varied (see Table S1). The analysis of the variance showed that the disruption location was the only disruption variable that had a significant effect on all parameters a, b, and c (see Fig. S3; Table S2). We concluded that the behavior of a WDS

subject to a water leakage, as described by the beta recovery function, was mostly dependent on the location of the disruption, which therefore had the highest discriminatory power for node clustering.

Recovery Function Fitting and Node Clustering

In order to individualize the most critical nodes and prioritize the efforts in allocating recovery resources, the total performance loss under the disruption of node i was computed by substituting MOP in Eq. (1) with $\text{MOP}_d^{(i)}$:

$$\Delta^{(i)} = \int_0^{T_{rec}} \left[1 - \frac{1}{n}\sum_{i=1}^{n} \frac{d_i(t)}{D_i(t)}\right] dt \tag{8}$$

Based on Eq. (8), the q most critical nodes were identified as those associated with total performance losses in the upper quartile, i.e., $\{i{:}\Delta^{(i)} \geq Q_3\}$, where Q_3 was the upper quartile of $\{\Delta^{(1)}, \ldots, \Delta^{(n)}\}$.

In order to study the behavior of the system following a disruption, the beta recovery function in Eq. (2) was fitted to the average satisfied demand $\text{MOP}_d^{(i)}$ simulated under the disruption of node i by minimizing the residual sum of squares:

$$\min_{a,b,c} \sum_t \left\{ \text{MOP}_d^{(i)}(t) - \left[\text{TP} - a\frac{(b+c)^{b+c}}{b^b c^c} \left(\frac{t}{T_{rec}^{(i)}}\right)^b \left(1 - \frac{t}{T_{rec}^{(i)}}\right)^c \right] \right\}^2 \tag{9a}$$

$$\text{s.t. } 0 \leq a \leq 1, b, c \geq 0 \tag{9b}$$

where t was the time of observation and $T_{rec}^{(i)}$ was the time to recovery observed when node i was disrupted. We used the limited-memory Broyden-Fletcher-Goldfarb-Shanno algorithm with bound constraints (L-BFGS-B) to solve the optimization problem. The goodness of fit was assessed by the R^2. By solving the problem in Eq. (9) for the performance $\text{MOP}_d^{(i)}$ simulated under the disruption of each node, a set of parameters (a_i, b_i, c_i) could be associated to each critical node $i, i = 1, \ldots, q$.

The set of the estimated parameters $\{(a_1, b_1), \ldots, (a_q, b_q)\}$ was normalized and used as features for clustering the most critical nodes. The resulting classification represented clusters of nodes $\{C_1, \ldots, C_K\}$ whose disruptions caused similar WDS behaviors, according to the extent to which the system could absorb and adapt to their disruption.

Results and Discussion

Evaluation of the Fit of the Beta Model

Figs. 3(a and e) show the distribution of the R^2 statistic computed in the q most critical scenarios for *Net3* and *C-Town*, respectively. The beta model shows a better fit for the responses related to *Net3* than to *C-Town*. The goodness of fit improves in cases of severe performance losses (high a), due to the fact that the variance of the observed performance increases with the amount of performance lost. In fact, not only does the R^2 statistic penalizes low total variation, but the beta model is also best suited to represent severe disruptions, for which the variance of the observed performance is high. Specifically, the outliers for the case of *C-Town* are associated with responses characterized by a delayed but limited loss of performance. In these cases, the beta recovery function underestimates the observed MOP in the early stage of the disruption, but helps nevertheless to model the subsequent performance loss and recovery behavior.

The values a_i, b_i, and $\Delta^{(i)}$ associated with the critical scenario in which node i is disrupted, with $i = 1, \ldots, q$, are shown in Figs. 3(b–d and f–h) for *Net3* and *C-Town*, respectively. Interestingly, the nodes connecting the main water source to the rest of the network are not critical, because their demand is low and the water supply provided by the nearby water source and pumps helps to compensate for water loss.

The figures suggest some common response behaviors among the disruptions at the nodes. Specifically, some degree of correlation is observed between the parameters. Overall, high values of a, which characterize low absorptive capability, correspond to high values of b, which characterize high adaptive capability, suggesting a trade-off between different resilience objectives.

In order to further explore these relationships, the critical nodes are plotted in the parameter space, as shown in Figs. 4(a and e) for *Net3* and *C-Town*, respectively. *Net3* is characterized by higher a and b values than *C-Town*. The higher adaptive capability (higher b) displayed by *Net3* might be due to its higher reserve capacity to average demand ratio. Conversely, the lower adaptive capability (lower b) displayed by *C-Town* shows that the distributed water tanks do not help to compensate for the water lost during disrupted conditions. The lower absorptive capabilities (higher a) displayed by *Net3* could be related to its lower level of detail (*Net3* is a large-scale WDS at a low resolution, while *C-Town* is a small-scale WDS at a high resolution). In fact, while the effects of a disruption in *C-Town* are limited to the end-customer demand, a failure of a component of *Net3* may compromise the entire supply path (Diao et al. 2014) and consequently limit the effectiveness of recovery efforts.

Given these comparisons, the results show that a WDS can be more resilient than another with respect to one resilience objective, i.e., adaptive capability, and less resilient with respect to another, i.e., absorptive capability. Furthermore, the proposed $n-1$ analysis supports the study of the distribution of the resilience capabilities at a network component level. In both networks, high Δ values are associated with nodes characterized by either high a values or low b values, suggesting that severe total performance losses are due to the demand delivery service either dropping to critically low levels at some point of time, or suddenly dropping to the minimum level shortly after the start of the disruption.

Classification of Demand Nodes

In order to validate these observations, the critical nodes are clustered according to their associated parameters a and b. The results are reported in Figs. 4(b, c, f, and g) for *Net3* and *C-Town*, respectively. In the case of *Net3*, two clusters are enough to represent the nodes, as shown by the elbow of the sum of the squared distances of the nodes to their assigned centroid in Fig. 4(b). The two clusters differ in terms of PL, T_{str} and performance loss rate, as indicated by the parameters a and b, respectively. Therefore one cluster, labeled delayed-but-severe, represents nodes associated with high PL and long T_{str}. The other cluster, labeled sudden-but-limited, represents nodes associated with short T_{str} but limited PL.

In the case of *C-Town*, three clusters are used to represent the nodes. In fact, while the higher number of nodes of *C-Town* is reflected in a higher sum of the squared distances compared to *Net3*, the higher complexity and the diversified demand that characterize this network (Pagano et al. 2019) result in mainly three types of response behaviors. Therefore, in addition to the cluster labels identified for *Net3*, a third cluster, labeled delayed-and-limited, represents nodes associated with long T_{str} and limited PL.

Figs. 4(d and h) show the topologies of *Net3* and *C-Town*, respectively, where the nodes are colored according to their clusters. Previous studies partition water networks based on topological

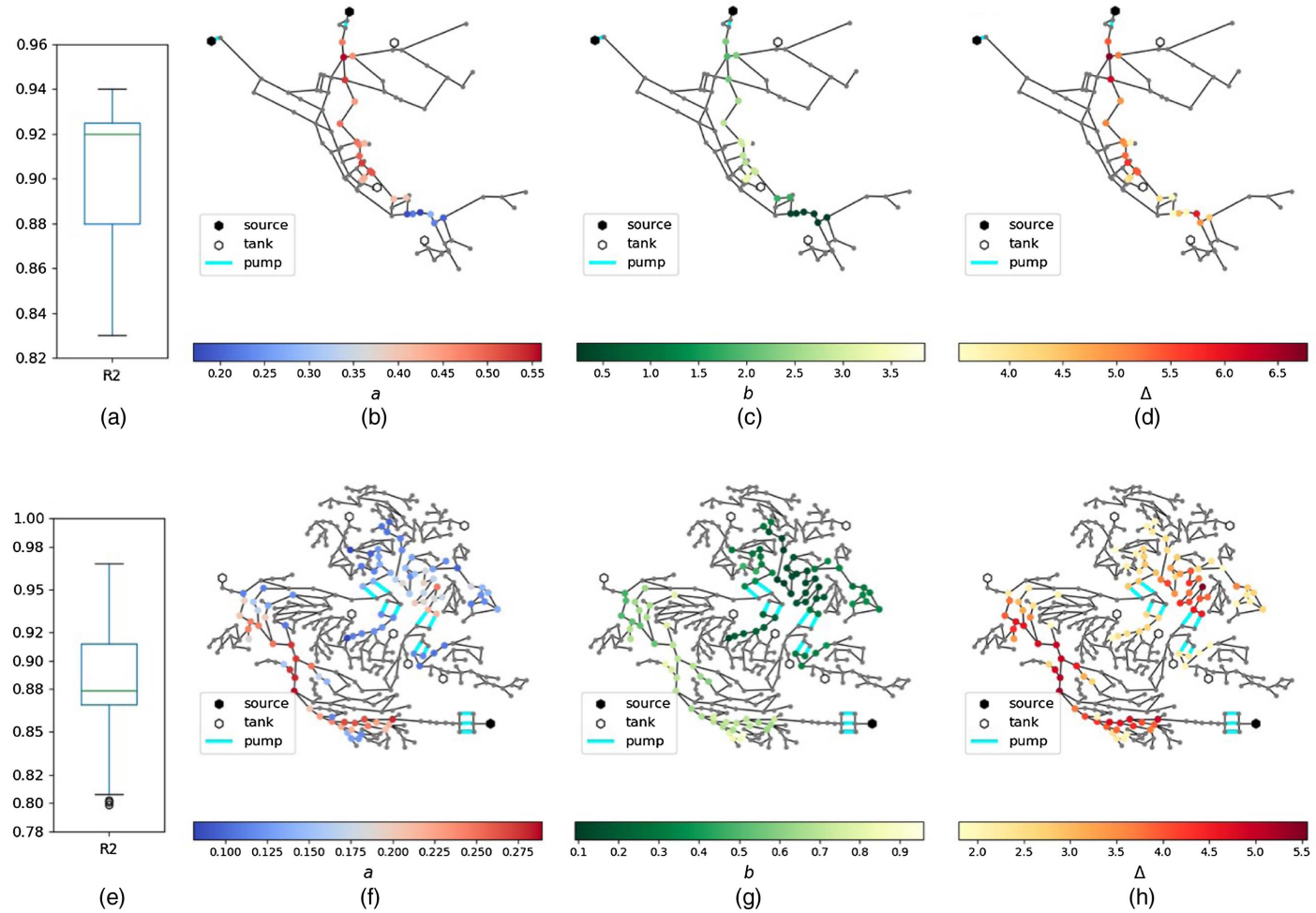

Fig. 3. Box plot of the goodness of fit statistic (R^2) for (a) *Net3*; and (e) *C-Town*. Topology of (b–d) *Net3*; and (f–h) *C-Town*, where each node is colored according to the estimated parameters a and b, and the total performance loss Δ.

information (Perelman and Ostfeld 2011; Diao et al. 2014; Di Nardo et al. 2018) or based on hydraulic behavior (Brentan et al. 2018), without reporting the results on the network topology. In contrast, in this paper the explanation of the results and the new findings are supported by two hybrid metrics, namely the connectivity to the source index (Herrera et al. 2015) and the demand adjusted entropic degree (Yazdani and Jeffrey 2012), which were computed for each node in the network (see Fig. S4). The connectivity to source index is inversely proportional to the energy loss associated with the supply of a node, and it is therefore a measure of its ease of supply. The demand adjusted entropic degree is proportional to the flow passing through a node, and it is therefore a measure of its criticality in satisfying the water demand of the connected nodes.

In both networks, the nodes labeled delayed-but-severe are located along the main path, connecting the primary water source to the demand nodes and consisting of pipes with large diameters (thick edges in the figures). In these cases, the high adaptive capability (long T_{str}) displayed by the WDSs suggests that the nominal demand delivery service can still be guaranteed thanks to the continuous water flow supplied by the water source. These nodes are in fact characterized by high connectivity to the source values, indicating that their ease of supply ensures their reliable operations. Accordingly, Wang and Au (2009) found that these nodes are the most reliable, since the chance of a disruption occurring on the path connecting them to the water source is relatively low. However, differing from other studies that simulated short disruptions (Diao et al. 2014; Meng et al. 2018), we find that the absorptive capability of the WDS associated with prolonged disruptions of these nodes is relatively low, since the depletion of the supply capacity of the water source leads to sudden drops of the demand delivery service until the point of reaching critically low levels. Accordingly, Herrera et al. (2015) showed that, for the case of *C-Town*, these nodes are dependent on the water reservoir, since there are no tanks in their proximity. The amount of performance loss is therefore proportional to the high flow passing though these nodes, as shown by their high demand adjusted entropic degree.

Conversely, the nodes labeled sudden-but-limited are located further away from the primary water source, but are critical to supplying water to peripheral nodes. In these cases, the low adaptive capability (short T_{str}) displayed by the WDSs suggests that the demand delivery service drops immediately following their disruption, since the peripheral nodes remain without supply of water. However, the loss of service is limited to the demand of the peripheral nodes, resulting in small PL.

For the case of *Net3*, nodes labeled sudden-but-limited are not identifiable through topology-based or hybrid metrics, as shown by the low values of the connectivity to the source index and demand adjusted entropic degree. The difficulty of supply associated with these nodes (low connectivity to the source index), which are further from the water sources and the water tanks, causes a sudden drop in performance following their disruption.

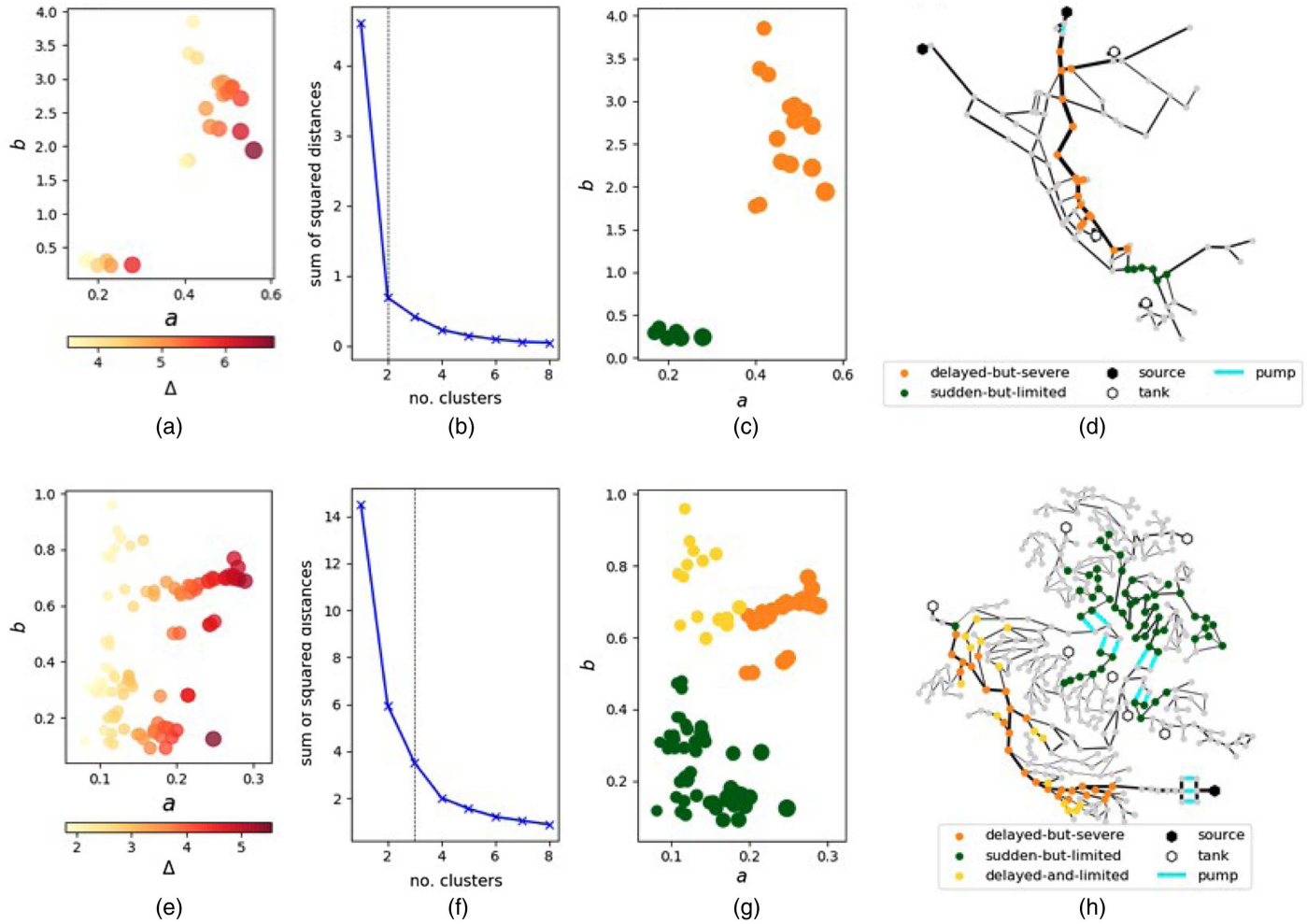

Fig. 4. Results for (a–d) *Net3*; and (e–h) *C-Town*. (a and e) Scatter plot displaying the nodes in the parameter space a and b. The size and the color of each node are proportional to the relative performance loss Δ. (b and f) Performance of the k-means algorithm. (c and g) Scatter plot displaying the nodes in the parameter space a and b. The size of each node is proportional to the relative performance loss Δ. The nodes causing the greatest performance losses ($\Delta \geq Q_3$) are colored according to their cluster. (d and h) Network topology where the nodes causing the greatest performance losses are colored according to their clusters. The thickness of the edges is proportional to the pipe diameter {diameter in [0.20 m, 2.51 m] (d) and in [0.05 m, 0.61 m] (h)}.

For the case of *C-Town*, nodes labeled sudden-but-limited partially overlap with nodes characterized by a relatively higher connectivity to the source index and demand adjusted entropic degree. A possible explanation for the sudden-but-limited behavior observed following their disruption might be found in the insufficient reserve capacity provided by the distributed water tanks. In fact, while the distributed water tanks are designed to meet the demand for water during normal operating conditions, their capacity might be inadequate to meet demand in the face of unexpected disruptions.

Hence, the proposed performance-based resilience assessment, although associated with a higher computational cost for solving the n hydraulic simulations, has proven effective in identifying disruptions scenarios with unusual recovery behaviors, i.e., slow performance losses followed by a sudden recovery, which could not be identified by topology-based metrics. These scenarios involve significant cumulative losses and therefore represent a fundamental lever to improve the resilience of a system.

Finally, for the case of *C-Town*, the nodes labeled delayed-and-limited include nodes with lower T_{str} and PL values, and for this reason characterized by lower Δ values. The response behavior of the WDS following their disruptions shares similarities with the cluster labeled delayed-but-severe, and strategies aimed at enhancing its resilience are expected to be effective also in this case.

Resilience Strategies

Node labels suggest areas for the improvement of the resilience of WDSs. For example, based on the expected time to strain T_{str} and the subsequent performance loss PL in the two clusters, system managers may prioritize and schedule repair sooner or later according to the criticality of the disrupted node. Strategies aimed at improving the absorptive capability of the WDS are to be put in place to address disruptions at the nodes labeled delayed-but-severe in order to limit performance loss. Conversely, strategies aimed at improving the adaptive capability of the WDS are to be put in place to address disruptions at the nodes labeled sudden-but-limited in order to delay the time to strain.

In the literature, various strategies were proposed to enhance WDS resilience, including increasing pipe diameter (Klise et al. 2017), pumping capacity (Chang and Shinozuka 2004; Cimellaro et al. 2015; Diao et al. 2016), and reserve capacity (Mugume et al. 2015). While optimization models were developed to find the best

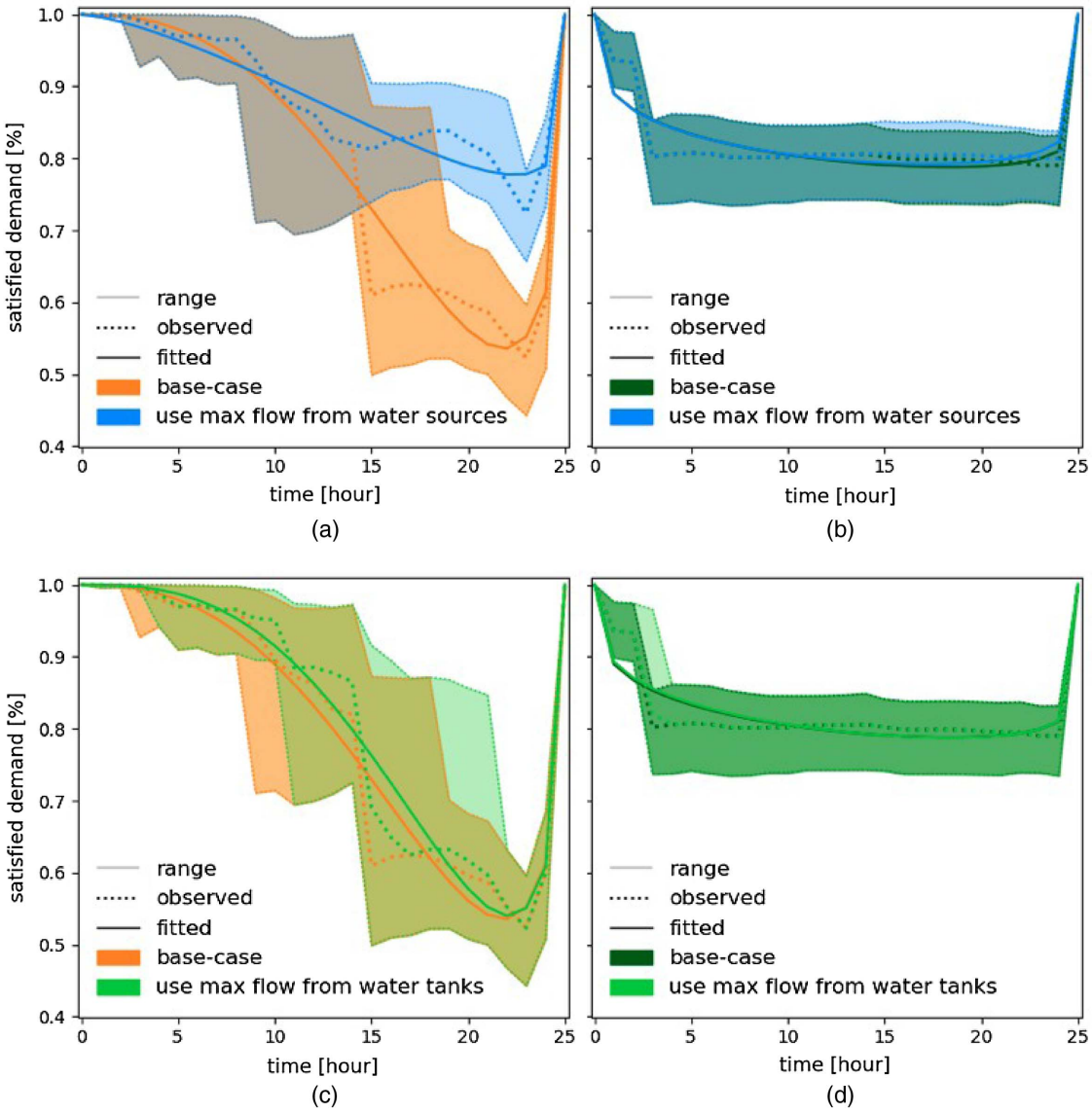

Fig. 5. Recovery strategies implemented on *Net3*: (a and b) response curve of the WDS when the maximum flow from the water sources is used and the nodes labeled delayed-but-severe (a) and sudden-but-limited (b) are disrupted. (c and d) Response curve of the WDS when the maximum flow from the water tanks is used and the nodes labeled delayed-but-severe (c) and sudden-but-limited (d) are disrupted.

strategies to improve system resilience under different disruption scenarios (Todini 2000; Jayaram and Srinivasan 2008; Creaco et al. 2016), the focus of this paper is to show how the proposed resilience assessment and $n-1$ analysis can inform the development of tailored strategies for improving distinct resilience objectives, i.e., absorptive and adaptive capabilities, under different disruption scenarios, i.e., disruption location.

For this purpose, the following two strategies are considered here: (1) using the maximum available flow from the water sources and (2) using the maximum available flow from the (increased-capacity) water tanks. For both networks, Strategy 1 is achieved by activating the pumps that operate the water sources during the entire duration of the disruption. For *Net3*, Strategy 2 is achieved by setting the minimum tank level, under which the tank stops the water supply, to zero. For *C-Town*, since the minimum tank level is zero in nominal conditions, Strategy 2 is achieved by increasing the diameter of the tanks by 20% and then activating the relative pumps during the entire duration of the disruption. The effects of the two resilience strategies are shown in Figs. 5 and 6 for the two networks. The values and associated statistics of the estimated parameters for the recovery functions fitted to the mean MOP_d under the different scenarios are reported in Tables 1 and 2. The estimated parameters are representative of the average behavior of the WDS according to the node cluster and implemented strategy and are therefore used for comparing the different scenarios.

For both networks, using the maximum flow from the water sources improves the absorptive capability, and it is therefore mostly beneficial when disruptions occur at the nodes labeled delayed-but-severe [Figs. 5(a) and 6(a)] or delayed-and-limited [Fig. 6(b)]. This is shown by the reduced values of the location parameter a, which characterizes absorptive capability, and the consequent reduction of the total performance loss Δ, which has maximum improvement for the nodes labeled delayed-but-severe (and delayed-and-limited) when this strategy is used (see values denoted with [a] and [b] in Tables 1 and 2).

Conversely, using the maximum flow from the water tanks improves the adaptive capability, and it is therefore mostly beneficial when disruptions occur at the nodes labeled sudden-but-limited

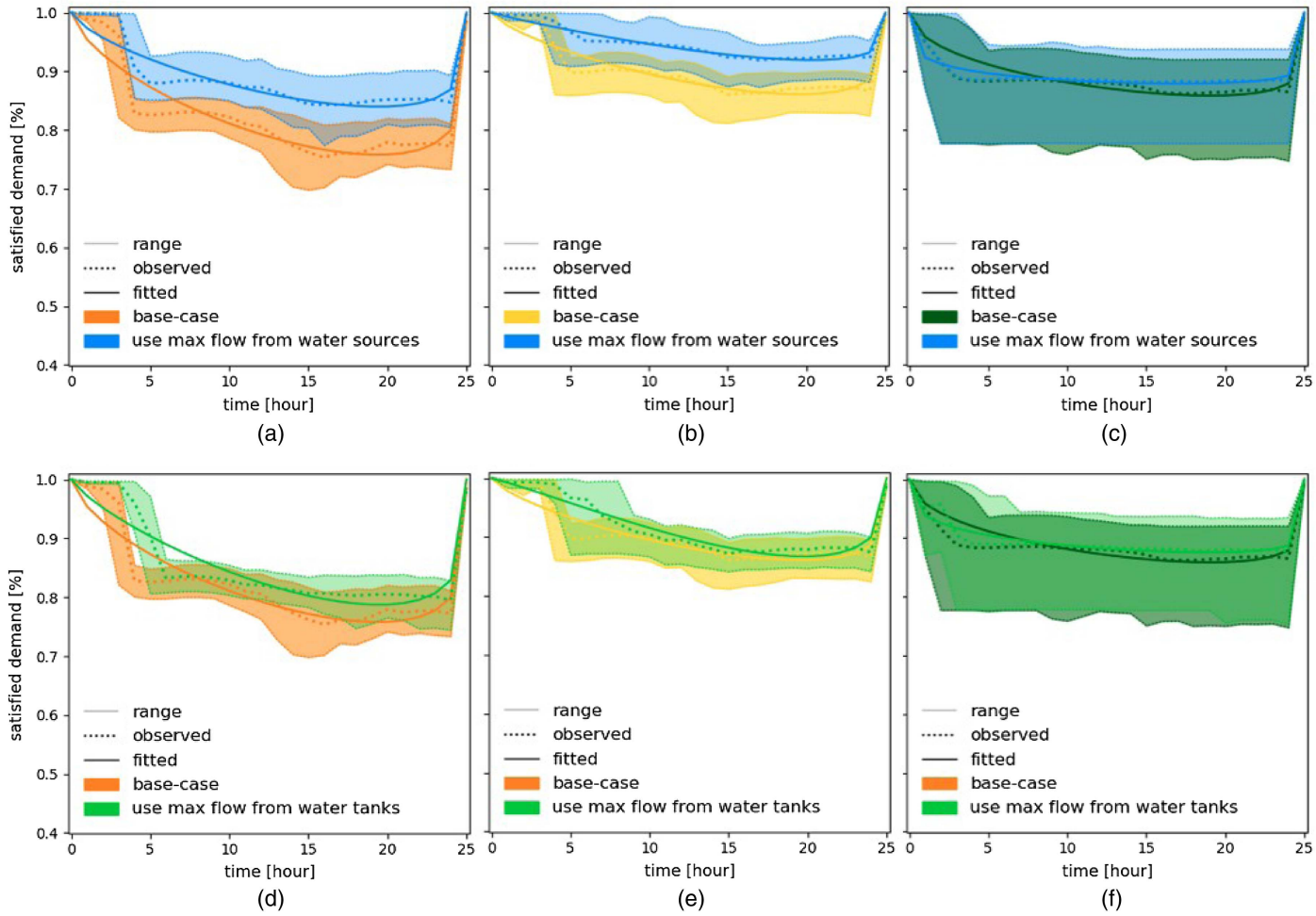

Fig. 6. Recovery strategies implemented on *C-Town*: (a–c) response curve of the WDS when the maximum flow from the water sources is used and the nodes labeled delayed-but-severe (a), delayed-and-limited (b), and sudden-but-limited (c) are disrupted; and (d–f) response curve of the WDS when the maximum flow from the water tanks is used and the nodes labeled delayed-but-severe (d), delayed-and-limited (e), and sudden-but-limited (f) are disrupted.

Table 1. Resilience assessment for *Net3*

Parameter	Delayed-but-severe	Sudden-but-limited
	Base-case scenario	
a	0.46	0.21
b	2.58	0.27
c	0.37	0.10
R^2	0.96	0.86
Δ	5.00	4.52
	Use max flow from water source	
a	0.22[a]	0.21
b	1.43	0.27
c	0.16	0.12
R^2	0.92	0.86
Δ	2.88[b]	4.45[b]
	Use max flow from water tanks	
a	0.46	0.21
b	2.92[c]	0.28[c]
c	0.38	0.10
R^2	0.96	0.88
Δ	4.60	4.50

[a]Denotes best improvement in parameter a.
[b]Denotes best improvement in Δ.
[c]Denotes best improvement in parameter b.

Table 2. Resilience assessment for *C-Town*

Parameter	Delayed-but-severe	Delayed-and-limited	Sudden-but-limited
	Base-case scenario		
a	0.24	0.14	0.14
b	0.66	0.73	0.49
c	0.19	0.20	0.15
R^2	0.90	0.90	0.83
Δ	4.42	2.47	2.88
	Use max flow from water sources		
a	0.16[a]	0.08[a]	0.12
b	0.71	0.93	0.20
c	0.20	0.21	0.09
R^2	0.88	0.95	0.94
Δ	2.86[b]	1.32[b]	2.66
	Use max flow from (increased-capacity) water tanks		
a	0.21	0.13	0.12
b	0.80[c]	1.13[c]	0.28[c]
c	0.22	0.30	0.09
R^2	0.88	0.94	0.93
Δ	3.69	2.10	2.62[b]

[a]Denotes best improvement in parameter a.
[b]Denotes best improvement in Δ.
[c]Denotes best improvement in parameter b.

[Figs. 5(d) and 6(f)]. This is shown by the increased values of the shape parameter b, which characterizes adaptive capability, and the consequent reduction of the total performance loss Δ, which, for the case of *C-Town*, has maximum improvement for the nodes labeled sudden-but-limited when this strategy is used (see values denoted with [c] and [b] in Table 2). For the case of *Net3*, while this strategy does not result in the maximum improvement of the average Δ, it is nevertheless most beneficial in reducing losses under some disruption scenarios, as shown by the upper range of MOP_d in Fig. 5(f).

Conclusions and Future Research

In this paper, we developed a model to quantify the time-continuous system response during the entire duration of a disruption, including periods of loss and restoration of performance. Specifically, a recovery function was formulated ad hoc to model the water delivery service of a WDS subject to water leakages, i.e., the beta family of recovery functions, which can fit scenarios of slow loss of performance followed by a sudden recovery, and whose parameters can be used to characterize the absorptive, adaptive, and recovery capabilities of a WDS.

Compared to other metrics that quantified WDS resilience based on the performance observed at specific points of time, recovery functions enable comparison amongst responses linked with various disruptions and system configurations, since the function parameters are associated with key resilience properties. Moreover, different from existing recovery functions that could only model a limited number of response behaviors, the proposed function is suited for modeling system responses characterized by slow performance losses followed by a relatively faster recovery. The model was applied to two benchmark networks, *Net3* and *C-Town*, which differed in terms of scale and level of detail. The results showed that the proposed recovery function well fits the performance of WDSs under simulated disruptions, and that the estimated parameters suggested clusters of nodes with similar criticality, to be addressed by tailored resilience strategies. We therefore proposed two strategies: maximization of the available flow from the water sources/tanks, aimed at improving the absorptive and adaptive capability of the WDS when disruptions occurred in the identified clusters.

Although the proposed strategies have proven useful for improving the average satisfied demand when disruptions occurred in different clusters, they present some practical limitations. For example, by increasing water flow, the pressure inside the system might also increase, leading to potential water losses. In future research, other system performances should also be considered and resilience strategies evaluated based on their associated costs and feasibility. Furthermore, we assumed that repairs to leaking components were conducted without interrupting service, which might not always be possible. Therefore, in future research, other repair techniques that consider valve closure should also be performed.

Correlation with existing topology-based metrics showed that the proposed resilience assessment is effective in identifying disruptions scenarios with unusual recovery behaviors, i.e., slow performance loss followed by a sudden recovery, which would have not been detected using existing hybrid metrics. These results are essential for designing resilient WDSs by addressing system criticality with effective strategies. Moreover, resources can be efficiently allocated by developing tailored resilience strategies according to the disruption location. The methodology presented in this paper is general and can be applied to different water networks.

In future research, the proposed model will be used to assess the resilience of various WDSs with different topologies and attributes (e.g., node elevation, node demand, etc.). By systematically varying these variables and assessing resilience, the results presented here could be generalized and the key factors enabling resilience identified. For example, different scenarios will be built by using basic topologies in order to detect the effects of topology on system resilience. This analysis will inform the development of resilience strategies to enhance the absorptive, adaptive, and recovery capabilities of systems based on topology and unique attributes. Redundant links and buffer reserve or supply capacity, for example, could help a WDS to absorb and adapt to disruptions. Effective emergency routines, such as disconnecting failed components through the use of isolation valves, could prevent cascading failures during disruptions and accelerate recovery (Zhang et al. 2020). Therefore, the methodology proposed here could be used to set general guidelines and support decisions to improve resilience.

Data Availability Statement

The following data and code that support the findings of this study are available from the corresponding author upon reasonable request: (1) *Net3* and *C-Town* water network models in INP EPANET format, and (2) Python code generated to conduct the study.

Acknowledgments

The research was conducted at the Future Resilient Systems at the Singapore-ETH Centre (SEC), which was established collaboratively between ETH Zurich and the National Research Foundation Singapore. This research is supported by the National Research Foundation, Prime Minister's Office, Singapore under its Campus for Research Excellence and Technological Enterprise (CREATE) programme. In addition, this research was part of the DeSIRE-programme (Designing Systems for Informed Resilience Engineering) of the 4TU Centre for Resilience Engineering (4TU.RE) which is funded by the 4TU-programme High Tech for a Sustainable Future (HTSF).

Supplemental Materials

Tables S1 and S2 and Figs. S1–S4 are available online in the ASCE Library (www.ascelibrary.org).

References

Amarasinghe, P., A. Liu, P. Egodawatta, P. Barnes, J. McGree, and A. Goonetilleke. 2016. "Quantitative assessment of resilience of a water supply system under rainfall reduction due to climate change." *J. Hydrol.* 540 (Sep): 1043–1052. https://doi.org/10.1016/j.jhydrol.2016.07.021.

Aydin, N. Y. 2018. "Measuring topological and operational resilience and recovery of water networks for planning and management." In *Proc., World Environmental and Water Resources Congress 2018: Hydraulics and Waterways, Water Distribution Systems Analysis, and Smart Water*, 370–379. Reston, VA: ASCE.

Brentan, B., G. Meirelles, E. Luvizotto Jr., and J. Izquierdo. 2018. "Hybrid SOM + k-means clustering to improve planning, operation and management in water distribution systems." *Environ. Modell. Software* 106 (Aug): 77–88. https://doi.org/10.1016/j.envsoft.2018.02.013.

Bruneau, M., et al. 2003. "A framework to quantitatively assess and enhance the seismic resilience of communities." *Earthquake Spectra* 19 (4): 733–752. https://doi.org/10.1193/1.1623497.

Butler, D., S. Ward, C. Sweetapple, M. Astaraie-Imani, K. Diao, R. Farmani, and G. Fu. 2017. "Reliable, resilient and sustainable water management: The Safe & SuRe approach." *Global Challenges* 1 (1): 63–77. https://doi.org/10.1002/gch2.1010.

Cassottana, B., L. Shen, and L. C. Tang. 2019. "Modeling the recovery process: A key dimension of resilience." *Reliab. Eng. Syst. Saf.* 190 (Oct): 106528. https://doi.org/10.1016/j.ress.2019.106528.

Chang, S. E. 1998. "Direct economic impacts." In *Engineering and socioeconomic impacts of earthquakes*, 75–92. Buffalo, NY: Multidisciplinary Center for Earthquake Engineering Research, Univ. of New York at Buffalo.

Chang, S. E., and M. Shinozuka. 2004. "Measuring improvements in the disaster resilience of communities." *Earthquake Spectra* 20 (3): 739–755. https://doi.org/10.1193/1.1775796.

Cimellaro, G., A. Tinebra, C. Renschler, and M. Fragiadakis. 2015. "New resilience index for urban water distribution networks." *J. Struct. Eng.* 142 (8): C4015014. https://doi.org/10.1061/(ASCE)ST.1943-541X.0001433.

Cimellaro, G. P., A. M. Reinhorn, and M. Bruneau. 2010. "Seismic resilience of a hospital system." *Struct. Infrastruct. Eng.* 6 (1–2): 127–144. https://doi.org/10.1080/15732470802663847.

Comes, T., and B. Van de Walle. 2014. "Measuring disaster resilience: The impact of Hurricane Sandy on critical infrastructure systems." In Vol. 11 of *Proc., 11th Int. ISCRAM Conf.*, 195–204. Brussels, Belgium: ISCRAM Association.

Creaco, E., M. Franchini, and E. Todini. 2016. "Generalized resilience and failure indices for use with pressure-driven modeling and leakage." *J. Water Resour. Plann. Manage.* 142 (8): 04016019. https://doi.org/10.1061/(ASCE)WR.1943-5452.0000656.

Crowl, D. A., and J. F. Louvar. 2001. *Chemical process safety: Fundamentals with applications*. London: Pearson Education.

Davis, C. A. 2014. "Water system service categories, post-earthquake interaction, and restoration strategies." *Earthquake Spectra* 30 (4): 1487–1509. https://doi.org/10.1193/022912EQS058M.

Diao, K., R. Farmani, G. Fu, M. Astaraie-Imani, S. Ward, and D. Butler. 2014. "Clustering analysis of water distribution systems: Identifying critical components and community impacts." *Water Sci. Technol.* 70 (11): 1764–1773. https://doi.org/10.2166/wst.2014.268.

Diao, K., C. Sweetapple, R. Farmani, G. Fu, S. Ward, and D. Butler. 2016. "Global resilience analysis of water distribution systems." *Water Res.* 106 (Dec): 383–393. https://doi.org/10.1016/j.watres.2016.10.011.

Di Nardo, A., M. Di Natale, R. Gargano, C. Giudicianni, R. Greco, and G. F. Santonastaso. 2018. "Performance of partitioned water distribution networks under spatial-temporal variability of water demand." *Environ. Modell. Software* 101 (Mar): 128–136. https://doi.org/10.1016/j.envsoft.2017.12.020.

Herckis, C. 2018. "Understanding hot tapping and plugging as an effective procedure to facilitate relocation, repair, or modification of water infrastructure when uninterrupted operation is necessary." In *Proc., Pipelines 2018: Utility Engineering, Surveying, and Multidisciplinary Topics*, 63–73. Reston, VA: ASCE.

Herrera, M., E. Abraham, and I. Stoianov. 2015. "Graph-theoretic surrogate measures for analysing the resilience of water distribution networks." *Procedia Eng.* 119: 1241–1248. https://doi.org/10.1016/j.proeng.2015.08.985.

Jayaram, N., and K. Srinivasan. 2008. "Performance-based optimal design and rehabilitation of water distribution networks using life cycle costing." *Water Resour. Res.* 44 (1): W01417. https://doi.org/10.1029/2006WR005316.

Khatavkar, P., and L. W. Mays. 2019. "Resilience of water distribution systems during real-time operations under limited water and/or energy availability conditions." *J. Water Resour. Plann. Manage.* 145 (10): 04019045. https://doi.org/10.1061/(ASCE)WR.1943-5452.0001112.

Klise, K. A., M. Bynum, D. Moriarty, and R. Murray. 2017. "A software framework for assessing the resilience of drinking water systems to disasters with an example earthquake case study." *Environ. Modell. Software* 95 (Sep): 420–431. https://doi.org/10.1016/j.envsoft.2017.06.022.

Mabrouk, N., J.-D. Mathias, and G. Deffuant. 2010. "Computing the resilience of a wastewater treatment bioreactor." In *Proc., 2010 5th Int. Multi-Conf. on Computing on the Global Information Technology*, 185–188. New York: IEEE.

McReynolds, M. R., and T. Peng. 2012. "Meeting the challenge of pipeline emergency repair." In *Proc., Pipelines 2012: Innovations in Design, Construction, Operations, and Maintenance, Doing More with Less*, 118–127. Reston, VA: ASCE.

Meng, F., G. Fu, R. Farmani, C. Sweetapple, and D. Butler. 2018. "Topological attributes of network resilience: A study in water distribution systems." *Water Res.* 143 (Oct): 376–386. https://doi.org/10.1016/j.watres.2018.06.048.

Mugume, S. N., D. E. Gomez, G. Fu, R. Farmani, and D. Butler. 2015. "A global analysis approach for investigating structural resilience in urban drainage systems." *Water Res.* 81 (Sep): 15–26. https://doi.org/10.1016/j.watres.2015.05.030.

Pagano, A., C. Sweetapple, R. Farmani, R. Giordano, and D. Butler. 2019. "Water distribution networks resilience analysis: A comparison between graph theory-based approaches and global resilience analysis." *Water Resour. Manage.* 33 (8): 2925–2940. https://doi.org/10.1007/s11269-019-02276-x.

Perelman, L., and A. Ostfeld. 2011. "Topological clustering for water distribution systems analysis." *Environ. Modell. Software* 26 (7): 969–972. https://doi.org/10.1016/j.envsoft.2011.01.006.

Porse, E., and J. Lund. 2015. "Network analysis and visualizations of water resources infrastructure in California: Linking connectivity and resilience." *J. Water Resour. Plann. Manage.* 142 (1): 04015041. https://doi.org/10.1061/(ASCE)WR.1943-5452.0000556.

Reed, D. A., M. D. Powell, and J. M. Westerman. 2010. "Energy supply system performance for Hurricane Katrina." *J. Energy Eng.* 136 (4): 95–102. https://doi.org/10.1061/(ASCE)EY.1943-7897.0000028.

Shen, L., B. Cassottana, H. R. Heinimann, and L. C. Tang. 2020. "Large-scale systems resilience: A survey and unifying framework." *Qual. Reliab. Eng. Int.* 36 (4): 1386–1401. https://doi.org/10.1002/qre.2634.

Tarani, F., C. Arrighi, L. Carnevali, F. Castelli, and E. Vicario. 2019. *Flood resilience of a water distribution system*, 177–194. Cham, Switzerland: Springer.

Todini, E. 2000. "Looped water distribution networks design using a resilience index based heuristic approach." *Urban Water* 2 (2): 115–122. https://doi.org/10.1016/S1462-0758(00)00049-2.

Todman, L. C., F. C. Fraser, R. Corstanje, L. K. Deeks, J. A. Harris, M. Pawlett, K. Ritz, and A. Whitmore. 2016. "Defining and quantifying the resilience of responses to disturbance: A conceptual and modelling approach from soil science." *Sci. Rep.* 6 (1): 28426. https://doi.org/10.1038/srep28426.

Vugrin, E. D., D. E. Warren, and M. A. Ehlen. 2011. "A resilience assessment framework for infrastructure and economic systems: Quantitative and qualitative resilience analysis of petrochemical supply chains to a hurricane." *Process Saf. Prog.* 30 (3): 280–290. https://doi.org/10.1002/prs.10437.

Wang, Y., and S.-K. Au. 2009. "Spatial distribution of water supply reliability and critical links of water supply to crucial water consumers under an earthquake." *Reliab. Eng. Syst. Saf.* 94 (2): 534–541. https://doi.org/10.1016/j.ress.2008.06.012.

Woods, D. D. 2015. "Four concepts for resilience and the implications for the future of resilience engineering." *Reliab. Eng. Syst. Saf.* 141 (Apr): 5–9. https://doi.org/10.1016/j.ress.2015.03.018.

Yazdani, A., and P. Jeffrey. 2012. "Water distribution system vulnerability analysis using weighted and directed network models." *Water Resour. Res.* 48 (6): W06517. https://doi.org/10.1029/2012WR011897.

Yazdani, A., R. A. Otoo, and P. Jeffrey. 2011. "Resilience enhancing expansion strategies for water distribution systems: A network theory approach." *Environ. Modell. Software* 26 (12): 1574–1582. https://doi.org/10.1016/j.envsoft.2011.07.016.

Zhang, Q., F. Zheng, Q. Chen, Z. Kapelan, K. Diao, K. Zhang, and Y. Huang. 2020. "Improving the resilience of postdisaster water distribution systems using dynamic optimization framework." *J. Water Resour. Plann. Manage.* 146 (2): 04019075. https://doi.org/10.1061/(ASCE)WR.1943-5452.0001164.